Article

Influence of the Available Surface Area and Cell Elasticity on Bacterial Adhesion Forces on Highly Ordered Silicon Nanopillars

Patrick W. Doll,*,[||] Katharina Doll,[||] Andreas Winkel, Richard Thelen, Ralf Ahrens, Meike Stiesch,[||] and Andreas E. Guber[||]

Read Online

| ACCESS | | Metrics & More | | Article Recommendations | | Supporting Information |

ABSTRACT: Initial bacterial adhesion to solid surfaces is influenced by a multitude of different factors, e.g., roughness and stiffness, topography on the micro- and nanolevel, as well as chemical composition and wettability. Understanding the specific influences and possible interactive effects of all of these factors individually could lead to guidance on bacterial adhesion and prevention of unfavorable consequences like medically relevant biofilm formation. On this way, the aim of the present study was to identify the specific influence of the available surface area on the adhesion of clinically relevant bacterial strains with different membrane properties: Gram-positive *Staphylococcus aureus* and Gram-negative *Aggregatibacter actinomycetemcomitans*. As model surfaces, silicon nanopillar specimens with different spacings were fabricated using electron beam lithography and cryo-based reactive ion etching techniques. Characterization by scanning electron microscopy and contact angle measurement revealed almost defect-free highly ordered nanotopographies only varying in the available surface area. Bacterial adhesion forces to these specimens were quantified by means of single-cell force spectroscopy exploiting an atomic force microscope connected to a microfluidic setup (FluidFM). The nanotopographical features reduced bacterial adhesion strength by reducing the available surface area. In addition, the strain-specific interaction in detail depended on the bacterial cell's elasticity and deformability as well. Analyzed by confocal laser scanning microscopy, the obtained results on bacterial adhesion forces could be linked to the subsequent biofilm formation on the different topographies. By combining two cutting-edge technologies, it could be demonstrated that the overall bacterial adhesion strength is influenced by both the simple physical interaction with the underlying nanotopography and its available surface area as well as the deformability of the cell.
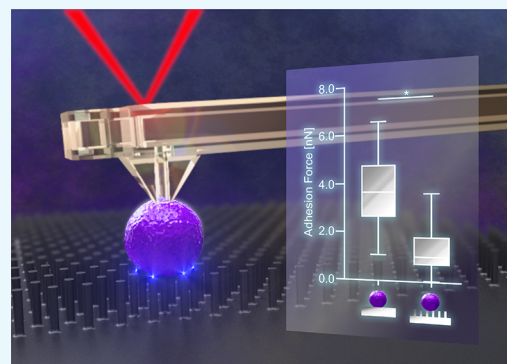
1. INTRODUCTION

Bacteria are prokaryotic single-cell organisms that can be found ubiquitous in nature. They have the capability to adhere to almost any material. When bacteria come into close proximity, they are passively attracted onto the surface.[1] Upon direct contact, specific adhesion structures on the bacterial membrane enable a stable adhesion. They comprise active movable flagella, fimbriae, pili, fibrils, and membrane-attached or membrane-associated adhesion proteins. The interactions of these specific structures with the surface are in the beginning based on unspecific electrostatic forces but later consist of more stable and specific interactions, like hydrogen bonds, calcium bridges, and hydrophobic and acid–base interactions.[2-5] These processes are highly species-specific and depend also on the material's surface characteristics.

The adhesion of a bacterial cell to a surface leads to massive changes in its gene expression, inducing the formation of a biofilm.[6] Such three-dimensional bacterial agglomerates consist of surface-attached and intercellularly attached bacteria that are surrounded by a self-produced matrix made of extracellular polymeric substances.[7] Biofilm formation poses major problems

in technical systems but also in modern medicine infections, e.g., on medical implants,[8-10] as biofilms are inherently resistant to the host immune response and antibiotic therapy.[11] The key to preventing biofilm formation and the resulting complications is an in-depth understanding of bacterial adhesion as its initial factor.

A multitude of different factors, including surface roughness and stiffness, feature geometry on a nano/microscale, and the subsequent available surface area, as well as chemical surface composition, contribute to bacterial adhesion.[5] Even though their general influence is well-established,[5,12] the mechanisms that determine the specific interaction of every individual factor with bacteria are still controversially discussed. As an example, for nanotopography and the resulting available surface area, it

A
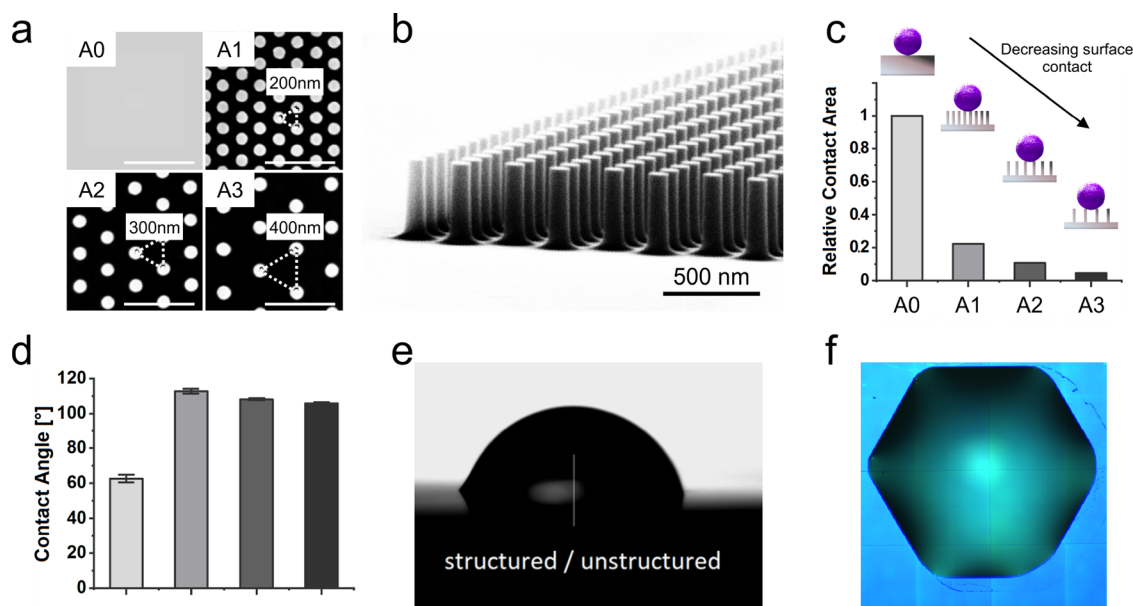
Figure 1. Results of sample characterization. (a,b) Scanning electron micrographs of fabricated nanopillar arrays with their geometrical configuration. A0, blank silicon surface; A1, hexagonal grid size of 200 nm; A2, 300 nm; A3, 400 nm. All pillar structures have nominal diameters of 100 nm and heights of 500 nm. (c) Resulting normalized available surface area on top of the structures. (d) Measured contact angles showing hydrophilic behavior on blank silicon (A0), while more hydrophobic behavior occurs on the structured samples (A1−A3). (e) Droplet placed on the transitional area of the structured and unstructured areas to demonstrate the resulting meniscus in the three-phase interface indicating movement due to nanocapillary forces. (f) Light microscopic image of a droplet taking a hexagonal shape, induced by the underlying nanotopography.

could be shown that increasing surface roughness and structures with feature sizes similar to bacteria support bacterial colonization.[5,13] However, there are also studies that showed an increased bacterial attachment on rough nanosurfaces[14,15] and others that demonstrated a reduced bacterial load on bacterium-sized topographies.[16,17] Often, the problem in analyzing the influence of an individual factor is that the analyzed surfaces vary in more than one parameter, making clear conclusions difficult. The precise and exclusive change of individual parameters and the detailed elucidation of their function in bacterial adhesion have not been the focus of research so far, also due to limited experimental possibilities.[5]

As a step in this direction, the aim of the present study was to analyze the specific influence of the available surface area on the adhesion of two clinically relevant bacterial strains (*Staphylococcus aureus* (*S. aureus*) and *Aggregatibacter actinomycetemcomitans* (*A. actinomycetemcomitans*)) that are pathogens associated with different medical disciplines (endoprosthetics and dentistry, respectively) and also differ in their membrane properties (Gram-positive and Gram-negative, respectively) but share a similar coccoid morphology. For this purpose, two cutting-edge technologies were combined. Electron beam lithography allowed us to fabricate adequate amounts of large-scale highly ordered silicon nanopillar arrays as model surfaces with different spacings keeping all other parameters constant. For the analysis of bacterial adhesion, force spectroscopy using an atomic force microscope connected to a microfluidic system (FluidFM) was applied to determine bacterial adhesion forces on the different nanostructured samples on a single-cell level with comparable high throughput. Furthermore, the effect of this initial interaction on bacterial attachment and subsequent biofilm formation was analyzed by means of viability staining and confocal laser scanning microscopy. The results of this study provided insights into the species-specific interaction of single bacterial cells with nanostructured surfaces differing in available

surface areas and, thus, can give new impulses for biofilm prevention and diagnosis.

2. RESULTS

2.1. Fabrication of Highly Ordered Silicon Nanopillar Arrays as Model Surfaces.
Using electron beam lithography, nanostructured surfaces with defined pillar arrangements were produced. The combination of an electron beam written mask with subsequent reactive ion etching allows for the fabrication of almost perfect nanoscale topographies with uniform surface characteristics in terms of surface chemistry and resulting roughness.[18,19] At least $N = 40$ samples per structure with comparable large structured fields of 5×5 mm^2 were produced. As illustrated in Figures 1a and 2b, all pillars had nominal diameters of 100 nm and heights of 500 nm. The pillar center-to-center distances were 200, 300, and 400 nm for A1, A2, and A3, respectively, arranged in an equidistant hexagonal grid. Consequently, the available surface area compared to the unstructured control surface A0 was reduced by approx. 77.3, 89.9, and 94.3% for A1, A2, and A3, respectively (Figure 1c).

To ensure high-quality samples for further analysis, the fabrication was optimized, and the resulting samples were characterized in detail. SEM images were used to quantify the average defect amount (e.g., missing pillars). It was determined to be 5.78×10^{-5} for the structure type A1, 2.20×10^{-6} for A2, and 3.92×10^{-6} for A3. Overall, the sample surfaces were nearly defect-free.

As shown in Figure 1d, the contact angle on bare silicon is stably hydrophilic at around 65°. The structured surfaces showed initial contact angles of about 117−108° with slightly falling tendencies when the pillars were placed more largely apart. Thus, when droplets were placed on the nanostructured surfaces, the resulting contact angles first showed hydrophobic behavior. However, it could be observed that instantly, a
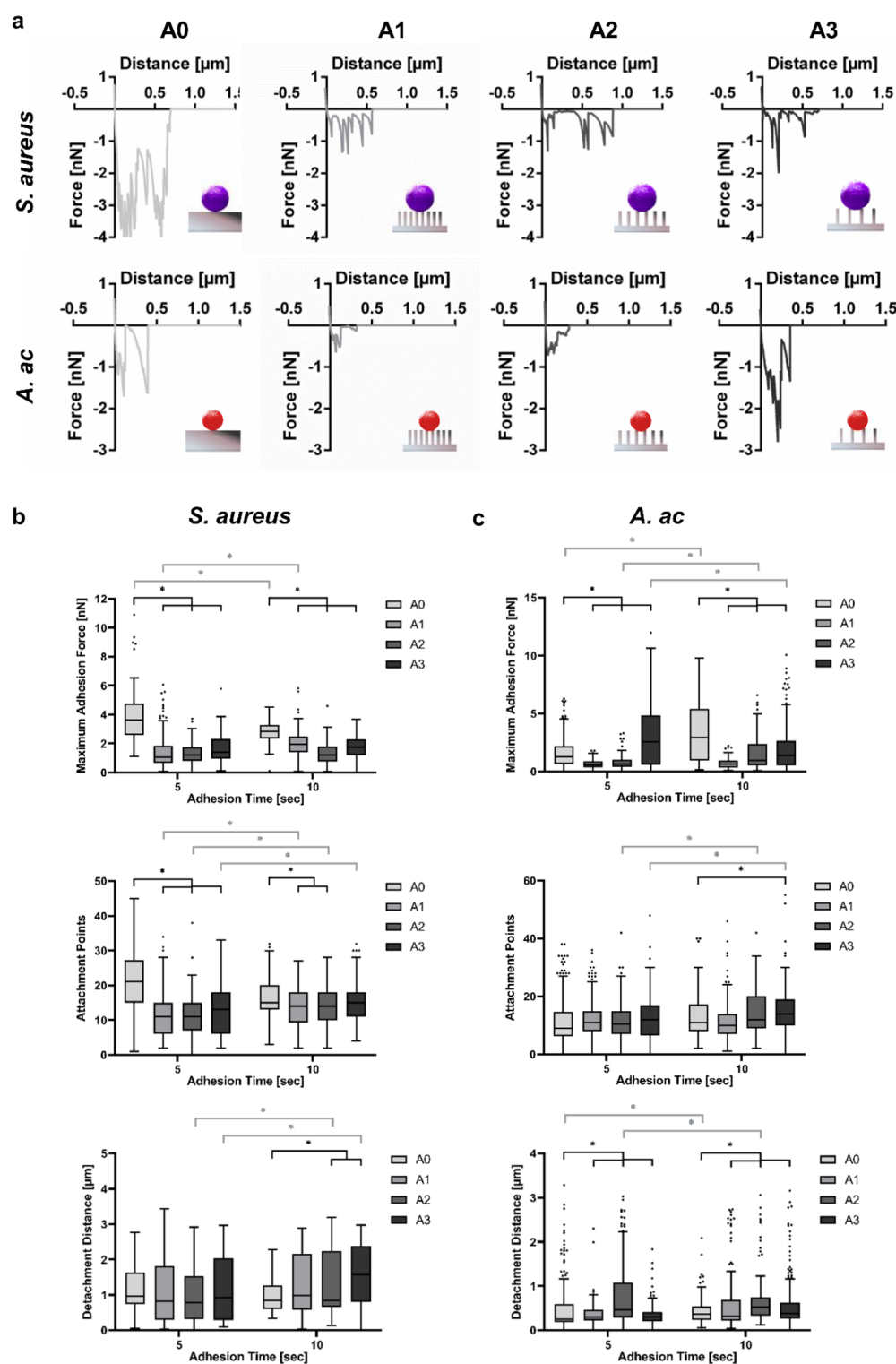
Figure 2. Bacterial single-cell adhesion forces on different nanotopographies. (a) Representative force−distance curves of single bacterial cells of indicated strains on different nanotopographies after a 5 s adhesion time. From force−distance curves after 5 and 10 s adhesion times, the deepest peak was quantified as the maximum adhesion force, the number of peaks as attachment points, and the distance until the curve returns to the baseline as the detachment distance. The results are given as Tukey boxplots for *S. aureus* (b) and *A. ac* (c). Asterisks (*) indicate statistically significant differences with $p \leq 0.05$ between groups (black brackets) and between time points (gray brackets).

transitional state builds up, pulling the droplet onto the surface. This could be recognized on all structured surfaces, while on the reference sample, the droplets held still. The resulting meniscus at the three-phase interphase indicated this movement (Figure 1e). If the droplet was observed from the top via light

microscopy, then the influences of nanotopography could also be visualized directly as it is demonstrated in Figure 1f. The droplets adopted a hexagonal shape due to the underlying nanotopography. This behavior intensified with an increased distance of the nanopillars.
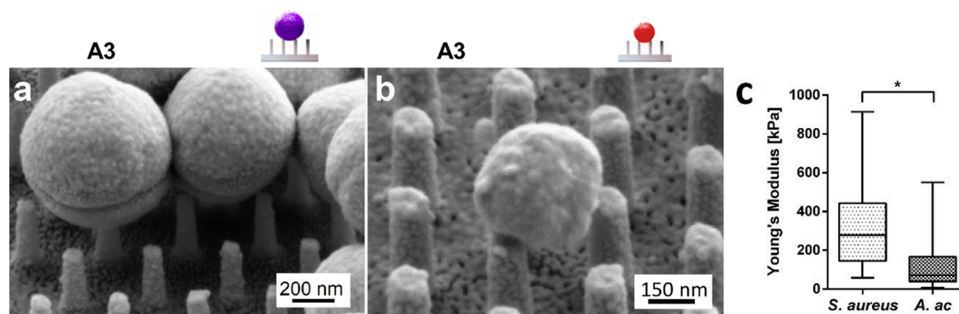
Figure 3. Interaction of bacteria with the nanostructured surfaces. SEM images of A3 structures demonstrate (a) rigid *S. aureus* sitting on top without any sign of deformation and (b) *A. ac* with a large deformation, partly sunken into the nanotopography. (c) Young's modulus for *S. aureus* and *A. ac* obtained from the approach force−distance curves reflecting the bacterial stiffness. The asterisk (*) indicates a statistically significant difference with $p \leq 0.05$.

2.2. Species-Specific Adhesion Forces on Nanostructured Surfaces.

To analyze the interaction of clinically relevant bacteria with different nanostructured surfaces on a single-cell level, the adhesion forces of *S. aureus* and *A. actinomycetemcomitans* (*A. ac*) were measured using single-cell force spectroscopy. These bacterial species where chosen to cover a wider range of relevance as they differ both in the related medical discipline and the membrane properties but exhibit a similar morphology. *S. aureus* is a Gram-positive, coccoid bacterium of approx. 1 μm diameter.[20] It is a common member of the healthy human skin and mucosa microbiome but also a major pathogen in implant-associated infections, especially in endoprosthetics. Mainly responsible for surface adhesion of *S. aureus* is a specific subset of single membrane proteins.[21,22] In contrast, *A. ac* is a Gram-negative cocco-bacillus with a size of approx. 0.4×1.0 μm.[23] It is an important pathogen in severe and recurrent oral periodontitis and could also be associated with peri-implantitis of dental implants.[24,25] The *A. ac* strain used for this study is defined as a "smooth" strain and, thus, also contains only adhesion molecules for surface adhesion.[23]

For single-cell force spectroscopy, a FluidFM system was used. Here, bacteria are not immobilized on the cantilever tip by drying or chemical fixation,[5] but the microfluidic system connected to the hollow cantilever allowed for a reversible physical immobilization by negative pressure. Even though diverse forces are applied to the bacterial cells and the geometry of cantilevers differs, the results of conventional force spectroscopy and FluidFM are comparable.[26] To ensure that only a single bacterium was measured, they were targeted individually under a microscope. Thus, efficient measurement of a comparable higher number of different bacterial cells (12 individual bacteria, each 16 times at different positions) in a native environment (e.g., in liquid) almost independently of their size, shape, and adhesion forces was possible.[27,28] The bacteria were placed on the surface with a gentle set point force of 0.75 nN to avoid bacterial compression and pressing them into the surface structures,[29] which would influence further analysis. Adhesion forces were measured after contact times of 5 and 10 s, and representative force−distance curves for a 5 s contact time on the different topographies are shown in Figure 2a. From these curves, the maximum adhesion force, the number of attachment points, and the detachment distance were quantified and further evaluated (Figure 2b,c).

For the maximum adhesion force, on the flat reference sample (A0), both strains exhibit comparable high maximum adhesion forces with average values of $3.94 \pm 1.90/2.80 \pm 0.73$ and $1.66 \pm 1.40/3.42 \pm 2.52$ nN for 5/10 s of adhesion of *S. aureus* and *A.*

ac, respectively. On the nanostructured surfaces, for both strains, a remarkable drop occurs already when surfaces with a 200 nm pillar distance (A1) were used. Here, statistically significant reductions in adhesion forces of approx. 30−80% at both contact times compared to the flat reference surfaces could be recognized. If the grid of the pillar arrangement is further increased to 300 (A2) or even 400 nm (A3), then the measured forces changed only slightly in comparison to A1. Only in the case of *A. ac* in contact with A3 for 5 s, a significantly higher adhesion force could be measured even exceeding the values related to A0. Notably, this effect was not observable for an extended contact time of 10 s.

For attachment points, similar to the values of maximum adhesion forces, for *S. aureus* also, the number of attachment points decreased on nanostructures in comparison to unstructured surfaces (A0). After a 5 s contact time, the reduction was approx. 50% and statistically significant for all structures (A1−A3). After 10 s, the reduction was limited to approx. 20% and only statistically significant in the case of A1 and A2. Between different nanostructures, no further statistically significant differences could be observed. In contrast, with *A. ac*, no statistically significant differences according to the number of attachment points occurred on the different surfaces, except for A3 after a 10 s contact time. Here, the number of attachment points significantly increased compared to the control.

Regarding the detachment distance, for *S. aureus*, similar distances were detected on all surfaces after a 5 s contact time. After 10 s, detachment distances on A2 and A3 significantly increased compared to the control (A0). In contrast, for *A. ac*, the detachment distances after a 5 s contact time on A1 and A3 significantly decreased compared to A0, whereas the distances on A2 significantly increased. After a 10 s contact time, detachment distances for all surfaces significantly increased compared to the control surface.

2.3. Bacterial Elasticity Influences the Surface Interaction.

To analyze the interaction of bacteria and the nanotopographies in more detail, SEM images were taken, as depicted in Figure 3. Both strains were found to maximize their surface contact by sitting in the center between 2, 3, or even 4 pillars. While *S. aureus* can be observed to be rigid and not deformed keeping its original spherical shape, it mainly sits on top of the structures (A3) only in contact with parts of the pillar heads. *A. ac.*, instead, was observed to be largely deformed and even partly sunk into the nanotopography.

This observation is in line with the results of elasticity measurement (Figure 3c). The Young's modulus obtained from the approach force−distance curves on the unstructured
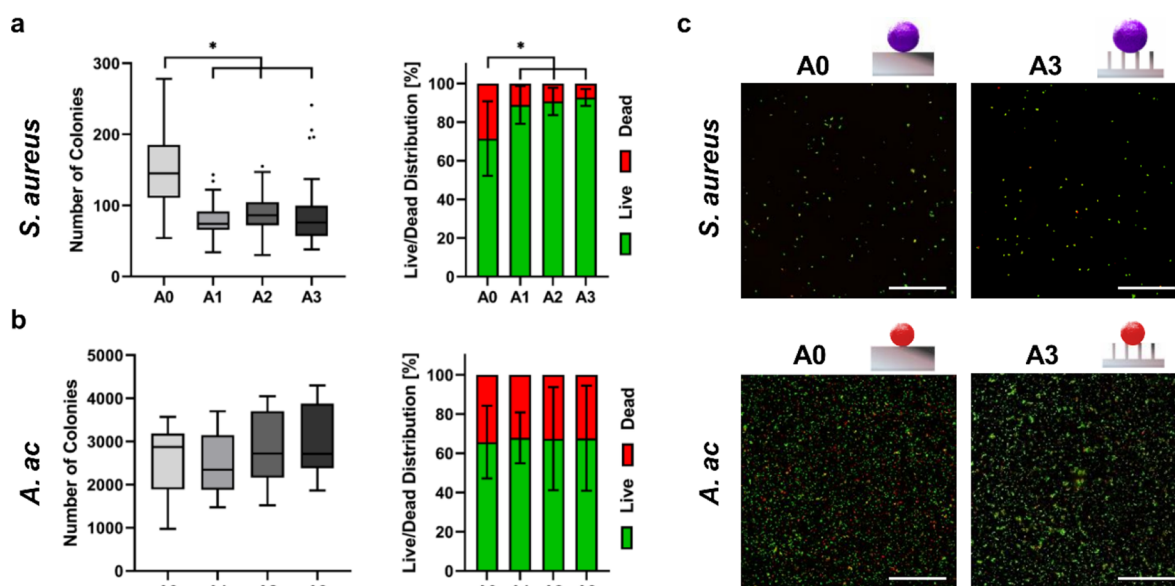
Figure 4. Initial bacterial attachment and viability after 5 h of incubation on different nanotopographies. Results are given as Tukey boxplots of attached colonies and the mean ± standard deviation of bacterial live/dead distribution for (a) *S. aureus* and (b) *A. ac*. Asterisks (*) indicate statistically significant differences with $p \leq 0.05$. In (c), representative microscopic images of initial attached bacterial cells are shown. Living bacteria are stained in green, whereas dead bacteria are stained in orange/red. Scale bars = 50 μm.
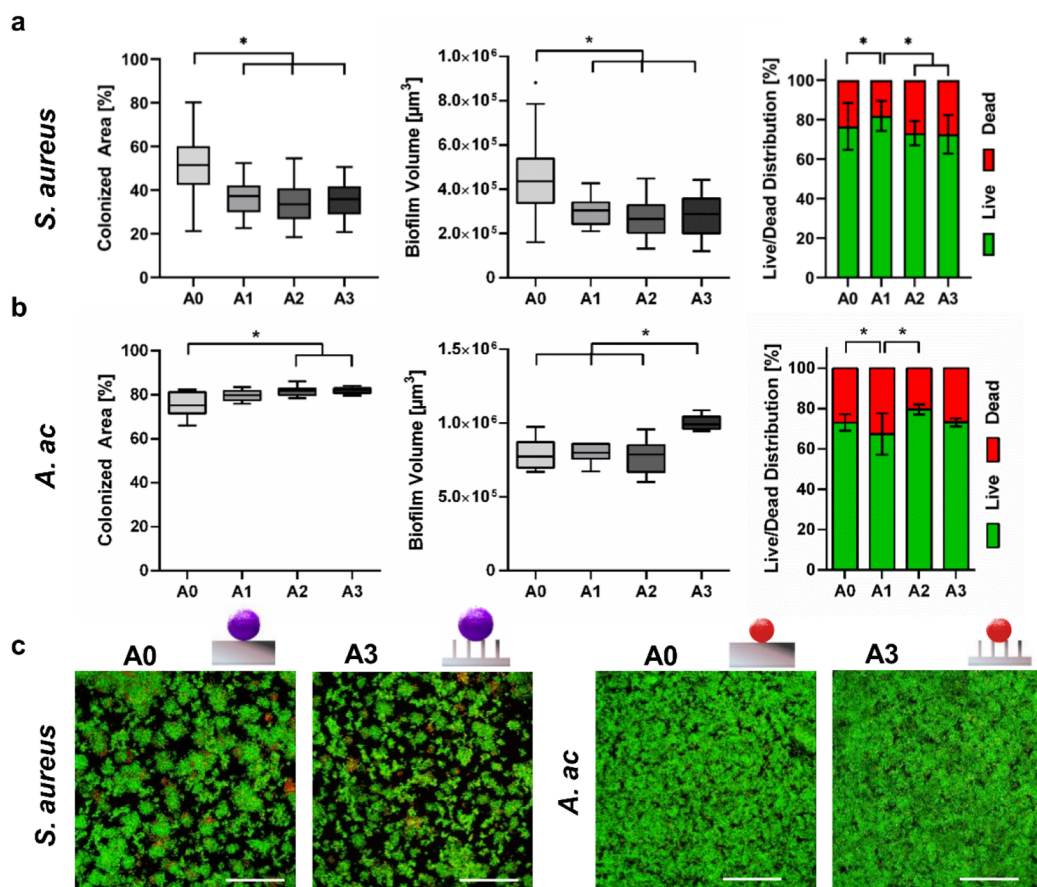
Figure 5. Bacterial biofilm formation and viability after 24 h of incubation on different nanotopographies. Results are given as Tukey boxplots of the colonized area by the biofilm and the biofilm volume and the mean ± standard deviation of bacterial live/dead distribution for (a) *S. aureus* and (b) *A. ac*. Asterisks (*) indicate statistically significant differences with $p \leq 0.05$. In (c), representative microscopic images of bacterial biofilms are shown. Living bacteria are stained in green, whereas dead bacteria are stained in orange/red. Scale bars = 50 μm.

reference surface A0 (Figure 1) reflects the bacterial stiffness. For *S. aureus*, a Young's modulus of approx. 320.4 kPa could be

measured. For *A. ac*, the Young's modulus, and thus the bacterial stiffness, was approx. three-fold lower with 108.4 kPa.

E

2.4. Species-Specific Initial Attachment to Nano-structured Surfaces. To investigate the consequences of the direct bacterial interaction with the surface, the influence of the different nanotopographies on bacterial initial attachment was analyzed microscopically after 5 h of incubation. The results are shown in Figure 4. The number of attached bacteria of *A. ac* is in general higher than that of *S. aureus*, which is due to the different optical densities required for successful cultivation of both strains.

For *S. aureus* (Figure 4a,c), the number of adhering bacterial colonies was significantly reduced by approx. 50% on all nanotopographies compared to the flat reference sample (A0). In contrast, the amount of living cells increased by approx. 20% on all nanotopographies compared to the flat reference sample. Between the different nanotopographies, there were no further significant differences in the number of adhering colonies or their viability.

For *A. ac* (Figure 4b,c), no significant differences between the nanotopographies and the flat reference sample could be detected, neither for the number of adhering colonies nor for the live/dead distribution. However, as the *p* values of the comparisons of A0/A3 and A1/A3 are only 0.122 and 0.294, respectively, whereas the *p* values of all other comparisons exceed 0.999, there might be a certain trend toward an increased initial attachment on A3.

2.5. Species-Specific Consecutive Biofilm Formation on Nanostructured Surfaces. To further analyze bacterial growth and biofilm formation on the different nanotopographies, attached bacteria were cultivated for a total of 24 h. After microscopic evaluation, the surface area covered by a biofilm, the biofilm volume, and the bacterial live/dead distribution were quantified and are shown in Figure 5. As for the quantification of initial attachment, the amount of the biofilm of *A. ac* is in general higher than that of *S. aureus*, which is again due to the different optical densities used and also due to different cultivation conditions (static vs shaking) applied. The respective conditions were selected to allow for the most stable and reproducible cultivation of both strains.

For *S. aureus* (Figure 5a,c), the area colonized by the biofilm and the biofilm volume were again significantly reduced by 30−40% on all nanotopographies compared to the flat reference surface (A0), whereas there were no differences within the nanotopographies. The biofilm viability was slightly but significantly increased on the surface with a 200 nm grid size (A1). However, the increase was only about 5%.

For *A. ac* (Figure 5b,c), the trend of increasing bacterial load observed for initial attachment could also be identified (approx. 5%) and reached statistical significance for the biofilm colonized area on the nanostructured surfaces with grid sizes of 300 and 400 nm (A2 and A3) compared to the flat reference surface. The effect was even more pronounced and reached significance for the biofilm volume on A3, where an approx. 25% increased volume compared to A0 could be detected. The biofilm volume on A2, as well as the colonized area and the biofilm volume on A1, showed no significant differences compared to the flat reference surface. Regarding biofilm viability, a slight but significant decrease in the amount of living cells could be observed on A1 compared to A0 and A2. However, this decrease was also only about 5%.

3. DISCUSSION

To gain a basic understanding of bacterial adhesion with regard to the specific influence of the underlying nanotopography and

the resulting available surface area, the present study analyzed single bacterial cell adhesion and subsequent biofilm formation to well-defined silicon nanopillar structures. For this purpose, sophisticated methods were needed that allow for fabrication of high-quality surface structures and efficient measurement of bacterial adhesion forces on a single-cell level.

Electron beam lithography offers the possibility to generate surface topographies in a highly ordered manner.[18] Almost any patterns, e.g., different lines, grids, or pillar arrangements, can be fabricated with the smallest tolerances and only very few defects. The generated nanotopographies A1, A2, and A3 were almost defect-free and showed the desired highly ordered pillar arrangement. Due to the fabrication process, the basic surface characteristics directly in contact with bacterial cells, i.e., surface chemistry and roughness, were uniform, whereas the available surface area continuously decreased. Also, surface wettability did not show large differences between the nanotopographies.

When analyzing the hydrophobicity of the nanostructured surfaces, the resulting contact angles first showed hydrophobic properties, which indicates a Cassie−Baxter state and a possible air layer trapped between the surface and the droplet. Yet, it could be observed that instantly, a transitional state (Wenzel state) builds up, pulling the droplet onto the surface. It can be assumed that there was no trapped air layer between the nanopillars, and due to nanocapillary forces, the droplets spread onto the surfaces. This phenomenon was observed for all different pillar arrangements and confirmed that bacteria were in direct contact to the nanotopographical features.

Taken together, electron beam lithography in combination with reactive ion etching enabled the fabrication of high-quality nanostructured surfaces. The different patterns only varied in their pillar distance and, thus, the available surface area, whereas all other parameters, like pillar geometry, surface roughness, and hydrophobicity, remained similar. This is in contrast to previous studies analyzing bacterial adhesion on nanostructured surfaces, where several parameters varied between the different surfaces.[5,30] Therefore, the test specimens of this study are particularly well-suited to act as model surfaces.

To analyze bacterial adhesion, AFM-based single-cell adhesion force spectroscopy was applied. In contrast to force spectroscopy, where a bulk of bacteria is coated on the cantilever tip and used for measurement, this method could account for single-cell-based heterogeneity in bacterial surface sensing, which is an important aspect in the development of micro-environments in biofilms.[31] The resulting force−distance curves consist of a major peak close to the surface (maximum adhesion force), which is mainly driven by electrostatic Lifshitz−van der Waals forces, and several minor peaks (attachment points), which represent specific hydrogen bonds.[32−34] *S. aureus* exhibited maximum adhesion forces, which are comparable to other studies.[29,35,39] The number of counted attachment points is less than that in a previous study by Aguayo et al.,[29] which is most probably due to a different bacterial strain used and their counting by worm-like chain modeling. Also, in the present study, no bond strengthening was observed for *S. aureus*. It describes an increase in adhesion forces over time upon removal of interfacial water molecules.[28,32] However, if compared to the literature, the extension of bond strengthening seems to depend on bacterial species and strains as well.[29,30] The detachment distance reflects bacterial and molecule stretching upon withdrawal.[29,32] As the distance detected for *S. aureus* in this study is quite long in comparison to previous studies,[29,35] it is more likely that here, some shearing of the bacterium over the

surface has been measured, too. For *A. ac*, bond strengthening could be observed from 5 to 10 s contact times. As this bacterium has not been subjected to single-cell force spectroscopy previously, a direct comparison of the adhesion force values is not possible, but they are within a common range observed for other bacterial species.[5] The same applies for the detected detachment distances.[29,35]

When the measured bacterial adhesion forces were linked to the present nanotopographical features, similar trends between the available surface area and the adhesion forces could be observed. With decreasing surface availability, bacterial adhesion forces decrease correspondingly. This principle could be observed for both strains, Gram-positive *S. aureus* and Gram-negative *A. ac*. As this phenomenon is also known from the literature,[30,36−38] the effect is more general and valid for larger groups of bacteria. Most probably, the reduced contact area on top of the pillars decreases electrostatic interactions between the bacterial membrane and the surface likewise, resulting in lower adhesion forces. Nevertheless, the influences of flagella and pili may be investigated in further studies as it is likely that such structures, which are not present in the bacterial species of this study, will change the adhesion drastically. In addition, the bacterial shape (spherical, rod-like, etc.) could also influence bacterial adhesion forces.

However, in addition to this simple physical influence, when analyzing the data in more detail, a more complex interaction between bacterial cells and nanotopographies beyond the available surface area can be revealed that also differs according to the bacterial strain.

For *S. aureus*, the maximum adhesion forces and the number of attachment points significantly decreased on the nanostructured surfaces compared to the flat control, yet no further decrease could be detected between the differently structured nanotopographies. Even though the difference between flat and structured surfaces got less pronounced when the contact time increased, the overall pattern did not change. This is in line with a previous study by Hizal et al., which focused on bacterial transmission between smooth and structured surfaces.[30] Additionally, an interaction occurs without larger cell deformation, as can be seen from the SEM images and the comparable higher Young's modulus and, thus, lower elasticity. Therefore, *S. aureus* adhesion seems to be quite opportunistic. With reduced surface availability, adhesion forces drop to a certain threshold but cannot be completely impaired (at least with the nanostructures of this study). The electrostatic interaction and adhesion proteins in the bacterial cell wall still seem to be sufficient to build up a stable connection to the features of the surface.[30] The details of this mechanism cannot be described by simple correlation to the available surface area and need to be investigated in further studies where comparable nanostructures with even less adhesion possibilities are used.

As *S. aureus*' initial attached cells and subsequent biofilm formation showed a similar pattern, reduced adhesion forces on the single-cell level are most likely also the reason for colonization behavior on the population level. The attachment pattern is also similar to that described by Linklater et al. on different nanopillared black silicon surfaces.[38] Bacterial cells on nanostructured topographies can more easily be removed, e.g., by washing procedures, than on the flat reference sample.[30] This is also supported by the increased viability observed on the structured samples. When adhesion forces are overall reduced, probably, only bacteria with intact membranes and, thus, adhesion molecules are able to remain on the surface, if shear forces are applied via fluid streams. In this regard, it should also be mentioned that the nanostructured surfaces of this study do not exhibit mechano-bactericidal effects as described for other nanopillars.[39,40] This is most likely due to the comparable lower aspect ratio of the topography and the high rigidity of the silicon surface. It has been shown that the bactericidal effect of nanopillars depends on a very high aspect ratio and is further supported by flexible pillars that bend upon bacterial contact and, thus, exert stress on the bacterial membrane.[5,41,42]

When comparing the results of Gram-positive *S. aureus* with those of Gram-negative *A. ac*, a clear drop in maximum adhesion strength on the nanostructured surfaces in comparison to the flat, unstructured surface could be seen as well. However, when the structure features are more largely apart, representing widths closer to the cell diameter, a large significant increase in the resulting adhesion strength could be observed after a contact time of 5 s. This effect gets reduced with time, but instead, the detachment distance increased on all surfaces. Compared to *S. aureus*, where also an increased detachment distance after prolonged contact time could be observed, the adhesion of *A. ac* overall seems to be more flexible. This is in line with the comparable higher elasticity and the visible deformation detected by SEM. It can be assumed that *A. ac* must have partly sunk into the gaps of the structure A3, increasing its surface contact and maximizing the resulting adhesion strength by means of additional shear forces on this structure type. A dependence of bacterial adhesion on elasticity, as well as an increased adhesion of more flexible bacterial cells, has been reported recently also for differently structured surfaces.[5,12] Interestingly, no differences in the number of attachment points could be observed for *A. ac*. As both strains only exhibit single adhesion molecules rather than larger structures like fimbriae or pili, this phenomenon has again to be attributed to the *A.ac* cell's greater flexibility. Most probably, the deformation of the cell wall allowed more molecules to bind to the surface and, thus, more easily compensated for the reduced surface available on all different structures. However, as for *S. aureus*, the detailed correlation of *A. ac*'s adhesion forces to the available surface area would require a more sophisticated mathematical study.

In contrast to *S. aureus*, the initial number of attached cells and the biofilm formation analyzed microscopically were not reduced for *A.ac*. Instead, there is a certain trend toward an increased initial adhesion and significantly more biofilm formation on the structure type A3. This indicates that the specific attachment points, which had not changed on the surfaces, are sufficient to attach the bacterium to the underlying substrate, even though the maximum adhesion force, which is attributed to electrostatic interactions, is decreased. If the bacterium probably sinks in between the structures, then not only the initial adhesion but also the biofilm formation increases.

4. CONCLUSIONS

In summary, the combination of cutting-edge technologies—electron beam lithography and single-cell force spectroscopy—allowed us to analyze the specific influences of a discrete nanotopography and its available surface area on bacterial adhesion without perturbation of further parameters. Bacterial adhesion on nanostructured surfaces in this study is influenced, on the one hand, by a simple physical interaction with the direct surface topography and its available surface area and, on the other hand, the elasticity and the deformability of the cell (Figure 6). The larger the deformability, the larger the adaptation to the surface topography.
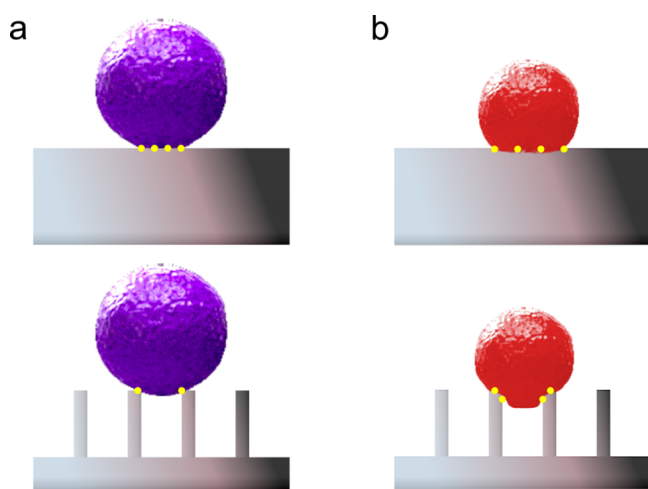
Figure 6. Schematic drawing of the interaction mechanisms of bacteria on nanotopographies. (a) Rigid and less deformable bacteria like Gram-positive *S. aureus* show less contact to the nanostructured surface. (b) A deformable cell like Gram-negative *A. ac* increases its surface interaction by deformation and partly adapting to the nanotopography. Yellow dots indicate adhesion points.

In the case of much less deformable Gram-positive *S. aureus*, it behaves like a rigid sphere on top of the structures and shows no considerable signs of deformation. In contrast, the more flexible Gram-negative *A. ac* shows an adaption to the structures and is, thus, able to increase its adhesion. The resulting adhesion forces are most probably the reason for the extension of subsequent biofilm formation.

The analyzed silicon nanopillar surfaces cannot be used as biofilm-inhibiting medical surfaces by themselves, first due to insufficient mechanical properties but also because they were not intended to. Yet, the knowledge gained through their analysis can serve as a basis for engineering sophisticated novel surfaces for various aspects in the field of biomedical science. By adaption of the underlying basic bacterial adhesion principles, a transfer to materials other than silicon, e.g., titanium or its alloys, can be achieved even with much simpler and cost-effective fabrication methods and even with arbitrary structures or patterns. Such a development will produce a novel generation of biomaterials with tailored surface properties to reduce adherent bacteria and subsequent biofilm formation and thereby might result in a reduction of biofilm-associated infections.

Bacterial adhesion is influenced by a multitude of different factors, not only the nanotopography and the available surface area. The approach of this study could further be used to decipher the influence of further surface parameters, e.g., roughness and hydrophobicity on bacterial adhesion, but also differences between bacterial strains of varying size and geometry. This could not only lead to a knowledge-based design of nanostructured surfaces that generally inhibit bacterial adhesion in real-life applications but could also set the basis for innovative diagnostic or preventive strategies. If the species-specific effect of nanotopographies can be confirmed on a larger scale, then this could be used, e.g., for selective prevention of pathogenic bacterial attachment or for fast on-site diagnostics.

5. MATERIALS AND METHODS

5.1. Sample Fabrication. *5.1.1. Electron Beam Lithography.* Nanostructured samples were fabricated by direct electron beam lithography and cryo-based dry etching as described earlier in detail.[18] Briefly, (100) silicon wafers were used as substrates and were first diced into 20×20 mm^2 chips. The diced wafers were scattered, and the individual chips were ultrasonically cleaned in acetone, 2-propanol (IPA), and deionized water (DI water), successively.

After substrate preparation, samples were coated with the negative-tone electron beam-sensitive photoresist hydrogen silsesquioxane (HSQ 6%, Dow Corning, Inc., USA) by spin-coating at a rotation speed of 3000 rpm and an acceleration ramp of 1500 rpm/s for 60 s (Opticoat, ATM GmbH, Germany). After the coating procedure, the samples were soft-baked for 60 s at 90 °C. Exposure was then carried out within the next 48 h.

Exposure was performed chip-based on a state-of-the-art electron beam pattern generator (EBPG5200Z, Raith GmbH, Dortmund, Germany). Up to 16 chips were exposed within one batch of fabrication, each with four individual structured fields with a size of 5×5 mm^2 each. The exposure strategy was highly optimized as described earlier in detail to reduce the necessary writing time.[18]

Four different layouts were exposed. For the flat reference surface (A0), a large beam step size and beam current were used. The different pillar arrangements were designed in the tightest packed hexagonal arrangement of different grid sizes while keeping the pillars' diameter constant at 100 nm. For the group termed A1, a center-to-center distance (grid size) of 200 nm was used, for A2 a grid size of 300 nm, and for A3 a grid size of 400 nm. All samples were fabricated by direct electron beam lithography and dry etching to assure best-quality samples with very low defect sizes and amounts.

After exposure, samples were manually developed in a 25% tetra-ammonium hydroxyl (TMAH) solution (BASF AG, Ludwigshafen, Germany) within a glass beaker for 120 s on a shaking plate at 150 rpm. The samples were then immediately rinsed with IPA followed by DI water for at least 30 s and finally dried with compressed nitrogen.

5.1.2. Reactive Ion Etching. After exposure and development, the samples were dry etched using a sulfuric hexafluoride (SF$_6$), oxygen (O$_2$), and argon (Ar$_2$) etching gas mixture within a cryo-based reactive ion etching process (Plasmalab 100/ICP 380, Oxford Instruments, Abingdon, Great Britain). The process started with an ignition step at a 1000 W inductively coupled plasma (ICP) power and a 100 W radio frequency (RF) power, for 4 s with the mentioned gas mixture. Afterward, the main etching step was carried out at a reduced ICP power for better etching rate control (700 W). The gas mixture was set to 20 sccm SF$_6$, 10 sccm O$_2$, and 10 sccm of Ar$_2$ at −110 °C to assure rectangular etching profiles and low side wall roughness values. Etching delivered approx. 500 nm in height. After the dry etching process, HSQ-glass masks were removed by wet etching using a buffered hydrofluoric acid (HF) solution (BOE) for 30 s. Finally, the samples were placed upside down in a special holder, laser cut, and manually divided into four pieces of 10×10 mm^2 each. The individual samples were then subsequently rinsed with acetone, IPA, and DI water and dried with compressed nitrogen.

5.2. Sample Characterization. *5.2.1. Scanning Electron Microscopy.* Fabricated samples were analyzed by scanning electron microscopy (SEM) (Supra 60 VP, Zeiss AG, Oberkochen, Germany). Extra high tensions (EHT) between 1.5 and 10 kV were used at different working distances and different tilt angles between 0 and approx. 90°. A secondary electron (SE2) detector was used.

To estimate the average amounts of defects within the topographies, several samples out of different fabrication batches

were analyzed. On each sample, 25 individual images were acquired per structure field at a magnification of 1000×. The structured area (5 × 5 mm^2) was divided into 25 equidistant sectors, each sector was semiautomatically addressed within a meandered path, and images were taken. Afterward, the defects on all images were counted manually.

In addition to the optimization of fabrication, SEM analysis was performed for further analysis of the bacterial cell/surface interaction on a higher magnification at the interface. Incubated samples were fixed in 2.5% formaldehyde for 15 min and dehydrated in ethanol (25, 50, 75, 90, and 98%). Then, they were critical point dried (CPD300, Leica GmbH, Wetzlar, Germany). Afterward, samples were sputter-coated with an approx. 10 nm-thick gold—palladium layer. Images were taken as mentioned above using an SE2 detector at a working distance of approx. 2 mm and an EHT of 1.5 kV. Each structure field was divided into 16 individual areas, the center of each field was addressed via an automated XY-stage, and an image at a magnification of 1000× was acquired. Three samples per parameter were analyzed in detail. Additionally, several samples were analyzed tilted (30, 45, and nearly 90°) with larger working distances and necessarily higher EHTs to identify the cells' position on the nanopillars and the cells' morphology and to get further information about the interface and the interaction between cells and surfaces.

5.2.2. Contact Angle Measurements. Contact angles were acquired with the sessile drop method (OCA20, Data Physics GmbH, Filderstadt, Germany). For each group (A0, A1, A2, and A3), at least three measurements were performed, and the average values were determined with the resulting standard deviation. The measurement procedure was kept strictly in timing and performed by only one operator to reduce variation induced by airflow, evaporation, or by the operator. A droplet volume of 1 μL of deionized water was used. In addition, microscopic images were acquired to visualize the top-view shape of the droplets and their infiltration into the underlying nanotopography (i.e., the Cassie—Baxter or Wenzel state).

5.3. Biological Testing. *5.3.1. Bacterial Strains and Culture Conditions.* *Staphylococcus aureus* (*S. aureus*, DSM 799) was obtained from the German Collection of Micro-organisms and Cell Cultures (DSMZ, Braunschweig, Germany). *Aggregatibacter actinomycetemcomitans* (*A. ac*, MCCM 2474) was obtained from the Microbial Culture Collection Marburg (Marburg, Germany). The bacteria were stored at −80 °C as glycerol stocks and precultured for every experiment. *S. aureus* was cultivated in tryptone soy broth (Oxoid Limited, Hampshire, UK) supplemented with 10% yeast extract (Carl Roth GmbH + Co. KG, Karlsruhe, Germany) continuously shaken under aerobic conditions at 37 °C for 16 h. *A. ac* was cultivated in Todd Hewitt broth (Oxoid Limited) supplemented with 10% yeast extract continuously shaken under micro-aerophilic conditions at 37 °C for 24 h.

5.3.2. Bacterial Single-Cell Force Spectroscopy. To obtain bacterial solutions for force spectroscopy, precultures were centrifuged, resuspended in filtered phosphate-buffered saline (Biochrom GmbH, Berlin, Germany), and adjusted to a theoretical optical density at 600 nm of 0.0005.

Force spectroscopy was performed as described previously using the FluidFM technology.[27] An atomic force microscope (AFM; FlexFPM, Nanosurf AG, Liestal, Switzerland) connected to a microfluidic pressure control system (Cytosurge AG, Zurich, Switzerland) was mounted on an inverse microscope (Eclipse Ti-S, Nikon GmbH, Düsseldorf, Germany). Hollow

silicon nitride cantilevers with a circular opening of 300 nm at the end and a theoretical spring constant of 0.6 N/m (FluidFM Nanopipette, Cytosurge AG) were used and connected to the microfluidic system. This allowed for reversible immobilization of single bacterial cells by applying negative pressure. Prior to every experiment, the exact spring constant of each cantilever was determined based on the method by Sader et al.;[43] it was always in the range of 0.6 ± 0.1 N/m. Cantilevers were filled with filtered, degassed phosphate-buffered saline, and the sensitivity was calibrated using machine software-implemented scripts.

The force spectroscopy setup exploited 50 mm glass dishes (WillCo Wells B.V., Amsterdam, The Netherlands) filled with the prepared bacterial suspension. To allow an at-grade insertion of test specimens, the dishes were equipped with a glass ring in advance. A single bacterial cell was targeted microscopically and captured with the approached cantilever on the glass ring with a set point force of 10 nN and a negative pressure of 400 mbar. The bacterium was transferred over the test specimen to perform single-cell force spectroscopy. On every surface, 12 individual bacterial cells were measured 16 times, each at different positions on the specimen. For this purpose, the bacterium was approached to the specimen's surface with a set point force of 0.75 nN, paused on the surface for 5 or 10 s with force feedback enabled, and retracted with a piezo velocity of 1 μm/s.

The resulting force—distance curves were analyzed with the software AtomicJ.[44] The settings are specified in Table S1. After quality control (e.g., to remove curves without surface contact), the maximum adhesion force, the number of attachment points, and the detachment distance were calculated from withdraw curves as illustrated in Figure 7. Bacterial elasticity was
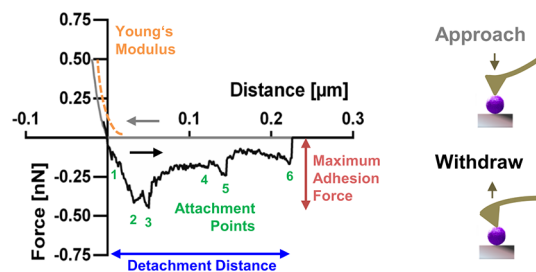
Figure 7. Schematic illustration of parameters quantified from force—distance curves of bacterial adhesion force spectroscopy.

quantified as the Young's modulus from the approach curves (Figure 7) on the flat reference surface A0 using the software-implemented Classical (L2) model (Table S1). GraphPad Prism software 8.4 (GraphPad Prism Software, Inc., La Jolla, USA) was used for data visualization and statistical analysis. After assessing the Gaussian distribution by D'Agostino—Pearson omnibus normality testing, significant differences to α = 0.05 were analyzed using the Kruskal—Wallis test with Dunn's multiple comparison correction for maximum adhesion forces and the number of attachment points as well as the Mann—Whitney test for Young's moduli.

5.3.3. Initial Attachment and Biofilm Formation. To analyze bacterial attachment and biofilm formation on nanotopographies, three individual precultures were centrifuged and resuspended in phosphate-buffered saline. They were adjusted to an optical density at 600 nm of 0.001 or 0.2 for *S. aureus* or *A. ac*, respectively. Test specimens (N = 18 per structure and strain) were incubated with bacterial suspensions using each

preculture in triplicates for 5 h at 37 °C and with continuous shaking under aerobic (in the case of *S. aureus*) or micro-aerophilic (5% CO_2, in the case of *A. ac*) conditions. After this initial attachment, half of the specimens ($N = 9$ per structure and strain) were processed for microscopy as described below.

On the other specimens, the bacterial suspension was removed and replaced with fresh medium: tryptone soy broth supplemented with 10% yeast extract and 50 mM glucose (Carl Roth GmbH & Co. KG) for *S. aureus* or Schaedler broth (Oxoid Limited) supplemented with 10 μg/mL vitamin K (Oxoid Limited) for *A. ac*. To allow for biofilm formation of the adhered cells, specimens were further incubated for a total of 24 h at 37 °C under aerobic conditions and continuous shaking in the case of *S. aureus* and under static microaerophilic conditions (5% CO_2) in the case of *A. ac*.

5.3.4. Fluorescence Staining and Microscopy. After initial attachment or biofilm formation, colonized specimens were rinsed two times with phosphate-buffered saline to remove unbound bacteria. Specimens were fluorescently stained using a LIVE/DEAD BacLight bacterial viability kit (Life Technologies, Darmstadt, Germany). Both fluorescent dyes, SYTO 9 and propidium iodide (PI), were applied simultaneously in a 1:2000 dilution in phosphate-buffered saline according to the manufacturer's instructions. Samples were fixed with 2.5% glutardialdehyde before being transferred to phosphate-buffered saline for microscopy. Bacterial colonization was examined by confocal laser scanning microscopy (CLSM, Leica TCS SP8, Leica Microsystems, Mannheim, Germany) using 488 and 552 nm excitation laser lines and emission spectra in the ranges of 500−550 (SYTO 9) and 600−700 nm (PI). For each specimen, five image stacks at different positions were taken with an area of $190 \times 190 \ \mu m^2$ and a z-step size of 2 μm.

The number of attached colonies and the live/dead distribution after initial attachment, as well as the biofilm surface colonization (proportion of the surface covered by bacteria), were quantified using ImageJ 1.48v software (Wayne Rasband, National Institutes of Health, USA, http://imagej.nih.gov/ij/). The 3D biofilm volume and the biofilm live/dead distribution were quantified using the Imaris 6.2.1 software package (Bitplane AG, Zurich, Switzerland). GraphPad Prism software 8.4 (GraphPad Prism Software, Inc.) was used for data visualization and statistical analysis. Gaussian distribution was assessed by D'Agostino−Pearson omnibus normality testing. According to the results, different tests to analyze significant differences to α = 0.05 were applied: the Kruskal−Wallis test with Dunn's multiple comparison correction for the numbers of attached colonies as well as *A. ac* biofilm surface coverage and the biofilm volume, ordinary one-way ANOVA with Tukey's multiple comparison correction for *S. aureus* biofilm surface coverage and the biofilm volume, and two-way ANOVA with Tukey's multiple comparison correction for all live/dead distributions.

5.3.5. Statistical Analysis. The software and statistical tests used for data visualization and evaluation are stated in the respective sections. Results are given as Tukey boxplots or the arithmetic mean $\pm$ standard deviation. Statistical significance was assessed at $p \leq 0.05$, which is referred to as "significant" in the Results and Discussion sections.

ASSOCIATED CONTENT

Supporting Information

The Supporting Information is available free of charge at https://pubs.acs.org/doi/10.1021/acsomega.2c00356.

Parameter settings for analysis of bacterial single-cell force spectroscopy force−distance curves using the software AtomicJ (PDF)

AUTHOR INFORMATION

Corresponding Author

Patrick W. Doll − *Institute of Microstructure Technology (IMT), Karlsruhe Institute of Technology (KIT), 76344 Eggenstein-Leopoldshafen, Germany;* orcid.org/0000-0001-9198-2756; Phone: +49 721 608-29317; Email: patrick.doll@kit.edu; Fax: +49 721 608-24331

Authors

Katharina Doll − *Department of Prosthetic Dentistry and Biomedical Materials Science, Hannover Medical School, 30625 Hannover, Germany; Lower Saxony Centre for Biomedical Engineering, Implant Research and Development (NIFE), 30625 Hannover, Germany;* orcid.org/0000-0002-4885-9821

Andreas Winkel − *Department of Prosthetic Dentistry and Biomedical Materials Science, Hannover Medical School, 30625 Hannover, Germany; Lower Saxony Centre for Biomedical Engineering, Implant Research and Development (NIFE), 30625 Hannover, Germany*

Richard Thelen − *Institute of Microstructure Technology (IMT), Karlsruhe Institute of Technology (KIT), 76344 Eggenstein-Leopoldshafen, Germany*

Ralf Ahrens − *Institute of Microstructure Technology (IMT), Karlsruhe Institute of Technology (KIT), 76344 Eggenstein-Leopoldshafen, Germany*

Meike Stiesch − *Department of Prosthetic Dentistry and Biomedical Materials Science, Hannover Medical School, 30625 Hannover, Germany; Lower Saxony Centre for Biomedical Engineering, Implant Research and Development (NIFE), 30625 Hannover, Germany*

Andreas E. Guber − *Institute of Microstructure Technology (IMT), Karlsruhe Institute of Technology (KIT), 76344 Eggenstein-Leopoldshafen, Germany*

Complete contact information is available at:
https://pubs.acs.org/10.1021/acsomega.2c00356

Author Contributions

‖P.W.D. and K.D. contributed equally to this work. Both working groups of M.S. and A.E.G. contributed equally to this work.

Author Contributions

P.W.D. and K.D. performed the conceptualization, methodologies, investigation, and original draft preparation. R.T., A.W., R.A., M.S., and A.E.G. reviewed and edited the manuscript. M.S. and AE.G. supervised the project.

Notes

The authors declare no competing financial interest.
The raw/processed data required to reproduce these findings can be shared on request to the corresponding author.

■ REFERENCES

(1) Flemming, H.-C.; Wingender, J. Biofilme — die bevorzugte Lebensform der Bakterien: Flocken, Filme und Schlämme. *Biol. Unserer Zeit* **2001**, *31*, 169−180.

(2) Nobbs, A. H.; Lamont, R. J.; Jenkinson, H. F. Streptococcus Adherence and Colonization. *Microbiol. Mol. Biol. Rev.* **2009**, *73*, 407.

(3) Huang, R.; Li, M.; Gregory, R. L. Bacterial interactions in dental biofilm. *Virulence* **2011**, *2*, 435−444.

(4) Hannig, C.; Hannig, M. The oral cavity—a key system to understand substratum-dependent bioadhesion on solid surfaces in man. *Clin. Oral Investig.* **2009**, *13*, 123−139.

(5) Elbourne, A.; Chapman, J.; Gelmi, A.; Cozzolino, D.; Crawford, R. J.; Truong, V. K. Bacterial-nanostructure interactions: The role of cell elasticity and adhesion forces. *J. Colloid Interface Sci.* **2019**, *546*, 192−210.

(6) O'Toole, G.; Kaplan, H. B.; Kolter, R. Biofilm formation as microbial development. *Annu. Rev. Microbiol.* **2000**, *54*, 49−79.

(7) Donlan, R. M. Biofilms Microbial Life on Surfaces. *Emerging Infect. Dis.* **2002**, *8*, 881−890.

(8) Romanos, G. E.; Javed, F.; Delgado-Ruiz, R. A.; Calvo-Guirado, J. L. Peri-implant diseases: a review of treatment interventions. *Dent. Clin. North Am.* **2015**, *59*, 157−178.

(9) Ahmed, S.; Darouiche, R. O. Anti-biofilm agents in control of device-related infections. *Adv. Exp. Med. Biol.* **2015**, *831*, 137−146.

(10) Dreyer, H.; Grischke, J.; Tiede, C.; Eberhard, J.; Schweitzer, A.; Toikkanen, S. E.; Glöckner, S.; Krause, G.; Stiesch, M. Epidemiology and risk factors of peri-implantitis: A systematic review. *J. Periodontal Res.* **2018**, *53*, 657−681.

(11) Davies, D. Understanding biofilm resistance to antibacterial agents. *Nat. Rev. Drug Discov.* **2003**, *2*, 114−122.

(12) Tamayo, L.; Melo, F.; Caballero, L.; Hamm, E.; Díaz, M.; Leal, M. S.; Guiliani, N.; Urzúa, M. D. Does Bacterial Elasticity Affect Adhesion to Polymer Fibers? *ACS Appl. Mater. Interfaces* **2020**, *12*, 14507−14517.

(13) Mitik-Dineva, N.; Wang, J.; Mocanasu, R. C.; Stoddart, P. R.; Crawford, R. J.; Ivanova, E. P. Impact of nano-topography on bacterial attachment. *Biotechnol. J.* **2008**, *3*, 536−544.

(14) Truong, V. K.; Lapovok, R.; Estrin, Y. S.; Rundell, S.; Wang, J. Y.; Fluke, C. J.; Crawford, R. J.; Ivanova, E. P. The Influence of Nano-Scale Surface Roughness on Bacterial Adhesion to Ultrafine-Grained Titanium. *Biomaterials* **2010**, *31*, 3674−3683.

(15) Ivanova, E. P.; Truong, V. K.; Wang, J. Y.; Berndt, C. C.; Jones, R. T.; Yusuf, I. I.; Peake, I.; Schmidt, H. W.; Fluke, C.; Barnes, D.; Crawford, R. J. Impact of nanoscale roughness of titanium thin film surfaces on bacterial retention. *Langmuir* **2010**, *26*, 1973−1982.

(16) Chung, K. K.; Schumacher, J. F.; Sampson, E. M.; Burne, R. A.; Antonelli, P. J.; Brennan, A. B. Impact of Engineered Surface Microtopography on Biofilm Formation of Staphylococcus Aureus. *Biointerphases* **2007**, *2*, 89−94.

(17) Doll, K.; Fadeeva, E.; Stumpp, N. S.; Grade, S.; Chichkov, B. N.; Stiesch, M. Reduced bacterial adhesion on titanium surfaces microstructured by ultra-short pulsed laser ablation. *BioNanoMaterials* **2016**, *17*, 53−57.

(18) Doll, P. W.; Al-Ahmad, A.; Bacher, A.; Muslija, A.; Thelen, R.; Hahn, L.; Ahrens, R.; Spindler, B.; Guber, A. E. Fabrication of silicon nanopillar arrays by electron beam lithography and reactive ion etching for advanced bacterial adhesion studies. *Mater. Res. Express* **2019**, *6*, 65402.

(19) Yang, J. K. W.; Cord, B.; Duan, H.; Berggren, K. K.; Klingfus, J.; Nam, S.-W.; Kim, K.-B.; Rooks, M. J. Understanding of hydrogen silsesquioxane electron resist for sub-5-nm-half-pitch lithography. *J. Vac. Sci. Technol., B* **2009**, *27*, 2622−2627.

(20) Hof, H.; Dörries, R. *Duale Reihe Medizinische Mikrobiologie: 6., unveränderte Auflage*, 6th ed.; Stuttgart, 2017.

(21) Foster, T. J. Surface Proteins of Staphylococcus aureus. *Microbiol. Spectrum* **2019**, *7*, DOI: 10.1128/microbiolspec.GPP3-0046-2018.

(22) Spengler, C.; Nolle, F.; Mischo, J.; Faidt, T.; Grandthyll, S.; Thewes, N.; Koch, M.; Müller, F.; Bischoff, M.; Klatt, M. A.; Jacobs, K.

(23) Inoue, T.; Shingaki, R.; Sogawa, N.; Sogawa, C. A.; Asaumi, J.-I.; Kokeguchi, S.; Fukui, K. Biofilm formation by a fimbriae-deficient mutant of Actinobacillus actinomycetemcomitans. *Microbiol. Immunol.* **2003**, *47*, 877−881.

(24) Fives-Taylor, P. M.; Meyer, D. H.; Mintz, K. P.; Brissette, C. Virulence factors of Actinobacillus actinomycetemcomitans. *Periodontol. 2000* **1999**, *20*, 136−167.

(25) Mombelli, A.; Décaillet, F. The characteristics of biofilms in peri-implant disease. *J. Clin. Periodontol.* **2011**, *38*, 203−213.

(26) Hofherr, L.; Müller-Renno, C.; Ziegler, C. FluidFM as a tool to study adhesion forces of bacteria - Optimization of parameters and comparison to conventional bacterial probe Scanning Force Spectroscopy. *PLoS One* **2020**, *15*, No. e0227395.

(27) Doll, K.; Yang, I.; Fadeeva, E.; Kommerein, N.; Szafrański, S. P.; Bei der Wieden, G.; Greuling, A.; Winkel, A.; Chichkov, B. N.; Stumpp, N. S.; Stiesch, M. Liquid-Infused Structured Titanium Surfaces: Antiadhesive Mechanism to Repel Streptococcus oralis Biofilms. *ACS Appl. Mater. Interfaces* **2019**, *11*, 23026−23038.

(28) Potthoff, E.; Ossola, D.; Zambelli, T.; Vorholt, J. A. Bacterial adhesion force quantification by fluidic force microscopy. *Nanoscale* **2015**, *7*, 4070−4079.

(29) Aguayo, S.; Donos, N.; Spratt, D.; Bozec, L. Nanoadhesion of Staphylococcus aureus onto Titanium Implant Surfaces. *J. Dent. Res.* **2015**, *95*, 1078−1084.

(30) Hizal, F.; Choi, C.-H.; Busscher, H. J.; van der Mei, H. C. Staphylococcal Adhesion, Detachment and Transmission on Nanopillared Si Surfaces. *ACS Appl. Mater. Interfaces* **2016**, *8*, 30430−30439.

(31) Ren, Y.; Wang, C.; Chen, Z.; Allan, E.; van der Mei, H. C.; Busscher, H. J. Emergent heterogeneous microenvironments in biofilms: substratum surface heterogeneity and bacterial adhesion force-sensing. *FEMS Microbiol. Rev.* **2018**, *42*, 259−272.

(32) Aguayo, S.; Donos, N.; Spratt, D.; Bozec, L. Probing the nanoadhesion of Streptococcus sanguinis to titanium implant surfaces by atomic force microscopy. *Int. J. Nanomed.* **2016**, *11*, 1443−1450.

(33) Mei, L.; Ren, Y.; Busscher, H. J.; Chen, Y.; van der Mei, H. C. Poisson Analysis of Streptococcal Bond-strengthening on Saliva-coated Enamel. *J. Dent. Res.* **2009**, *88*, 841−845.

(34) Hermansson, M. The DLVO theory in microbial adhesion. *Colloids Surf., B* **1999**, *14*, 105−119.

(35) Alam, F.; Balani, K. Adhesion force of staphylococcus aureus on various biomaterial surfaces. *J. Mech. Behav. Biomed. Mater.* **2017**, *65*, 872−880.

(36) Yuan, Y.; Hays, M. P.; Hardwidge, P. R.; Kim, J. Surface characteristics influencing bacterial adhesion to polymeric substrates. *RSV Adv.* **2017**, *7*, 14254−14261.

(37) Tang, M.; Chen, C.; Zhu, J.; Allcock, H. R.; Siedlecki, C. A.; Xu, L.-C. Inhibition of bacterial adhesion and biofilm formation by a textured fluorinated alkoxyphosphazene surface. *Bioact. Mater.* **2021**, *6*, 447−459.

(38) Linklater, D. P.; Nguyen, H. K. D.; Bhadra, C. M.; Juodkazis, S.; Ivanova, E. P. Influence of nanoscale topology on bactericidal efficiency of black silicon surfaces. *Nanotechnology* **2017**, *28*, 245301.

(39) Ivanova, E. P.; Hasan, J.; Webb, H. K.; Gervinskas, G.; Juodkazis, S.; Truong, V. K.; Wu, A. H. F.; Lamb, R. N.; Baulin, V. A.; Watson, G. S.; Watson, J. A.; Mainwaring, D. E.; Crawford, R. J. Bactericidal activity of black silicon. *Nat. Commun.* **2013**, *4*, 2838.

(40) Hasan, J.; Raj, S.; Yadav, L.; Chatterjee, K. Engineering a nanostructured "super surface" with superhydrophobic and super-killing properties. *RSC Adv.* **2015**, *56*, 44953−44959.

(41) Ivanova, E. P.; Linklater, D. P.; Werner, M.; Baulin, V. A.; Xu, X.; Vrancken, N.; Rubanov, S.; Hanssen, E.; Wandiyanto, J.; Truong, V. K.; Elbourne, A.; Maclaughlin, S.; Juodkazis, S.; Crawford, R. J. The multi-faceted mechano-bactericidal mechanism of nanostructured surfaces. *PNAS* **2020**, *23*, 12598−12605.

(42) Singh, J.; Sharma, V.; Chandorkar, S.; Sen, P. *Bacterial Force on Nanopillars: Interaction at Single Cell, 2021 21st International Conference*

on Solid-State Sensors, Actuators and Microsystems (Transducers) 2021, 1040−1043.

(43) Sader, J. E.; Chon, J. W. M.; Mulvaney, P. Calibration of rectangular atomic force microscope cantilevers. *Rev. Sci. Instrum.* **1999**, *70*, 3967−3969.

(44) Hermanowicz, P.; Sarna, M.; Burda, K.; Gabryś, H. AtomicJ: an open source software for analysis of force curves. *Rev. Sci. Instrum.* **2014**, *85*, 63703.